Light-Induced Helix Movements in Channelrhodopsin-2

Maria Müller[1], Christian Bamann[2], Ernst Bamberg[2] and Werner Kühlbrandt[1]

1 - *Max Planck Institute of Biophysics Department of Structural Biology,* Max von Laue Strasse 3, 60438 Frankfurt, Germany
2 - *Max Planck Institute of Biophysics Department of Biophysical Chemistry,* Max von Laue Strasse 3, 60438 Frankfurt, Germany

Correspondence to Werner Kühlbrandt: werner.kuehlbrandt@biophys.mpg.de.
http://dx.doi.org/10.1016/j.jmb.2014.11.004
Edited by I. Shimada

Abstract

Channelrhodopsin-2 (ChR2) is a cation-selective light-gated channel from *Chlamydomonas reinhardtii* (Nagel G, Szellas T, Huhn W, Kateriya S, Adeishvili N, Berthold P, et al. Channelrhodopsin-2, a directly light-gated cation-selective membrane channel. Proc Natl Acad Sci USA 2003;100:13940–5), which has become a powerful tool in optogenetics. Two-dimensional crystals of the slow photocycling C128T ChR2 mutant were exposed to 473 nm light and rapidly frozen to trap the open state. Projection difference maps at 6 Å resolution show the location, extent and direction of light-induced conformational changes in ChR2 during the transition from the closed state to the ion-conducting open state. Difference peaks indicate that transmembrane helices (TMHs) TMH2, TMH6 and TMH7 reorient or rearrange during the photocycle. No major differences were found near TMH3 and TMH4 at the dimer interface. While conformational changes in TMH6 and TMH7 are known from other microbial-type rhodopsins, our results indicate that TMH2 has a key role in light-induced channel opening and closing in ChR2.

Introduction

Like other rhodopsins, channelrhodopsin-2 (ChR2) has seven transmembrane helices (TMHs) and a retinal chromophore forming a protonated Schiff base with the conserved Lys257 in TMH7 [2,3]. Upon light activation, the retinal isomerizes from the all-*trans* to the 13-*cis* form. Photoisomerization prompts conformational changes of the protein, which open the channel for cation translocation [4]. The cation flux in the conductive state of ChR2 depolarizes the cell membrane and, when expressed in neurons, triggers an action potential. This enables non-invasive investigation of neural circuits at high spatial and temporal resolution in optogenetics [5,6].

In order to understand the mechanism of light transduction by ChR2, it is necessary to determine how the protein structure changes at specific steps in the photocycle. Cryo-electron microscopy (EM) of two-dimensional (2D) crystals is the method of choice for investigating conformational changes in membrane proteins in response to light [7], ligands [8] or pH [9]. In this study, we investigate the slow C128T ChR2 mutant, which has an ~200 times longer lifetime of the open state than the wild-type [4,10,11]. This allowed us to trap defined functional states in the photocycle (Fig. 1).

Results and Discussion

2D crystals [2,3,12] diffracting to 6 Å resolution (Fig. 2A and B) yielded projection maps with density peaks characteristic of membrane-spanning helices (Fig. 2C). Based on the 2.3-Å X-ray structure of a channelrhodopsin-1/channelrhodopsin-2 chimera (C1C2) in the closed/dark-adapted state [4,13], we assigned the densities in the projection map to the seven TMHs in ChR2 (Fig. 3). Like ChR2, C1C2 is a dimer with TMH3 and TMH4 at the interface.

Projection difference maps, calculated by subtracting amplitudes and phases from different photocycle intermediates, revealed details of light-induced conformational changes in C128T ChR2. Figure 4A shows the difference map between the open and the closed/dark-adapted states. The closed state was
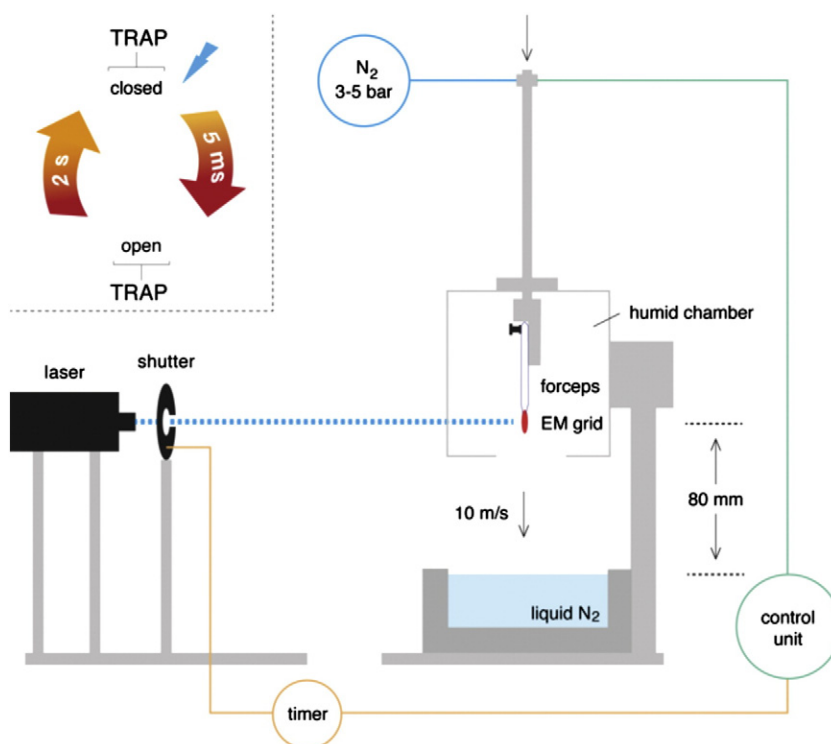
Fig. 1. Apparatus for trapping ChR2 photocycle intermediates. Left: diode-pumped solid-state laser (beam diameter, ~3 mm). Right: cryo-plunger. The shutter unit controls the exposure time of the blue laser pulse (λ_b = 473 nm; t = 0.5 s). With the end of the illumination, the plunger projects the grid into liquid nitrogen thereby trapping the illuminated state. Inset: main functional states in the C128T ChR2 photocycle initiated by blue light. The arrows indicate the transition time at 25 °C from the closed state to the open state and vice versa. Brackets: functional states of the trapped C128T ChR2 crystals.

obtained by incubating the 2D crystals in the dark (>12 h), after which samples were handled under red light (λ_r = ~750 nm). The open state was trapped by irradiating dark-adapted 2D crystals on the EM grid (λ_b = 473 nm; t = 0.5 s) and freeze-trapping the illuminated state by injecting the grid into liquid nitrogen within 120 ms (for more details, see Materials and Methods). This illumination protocol accumulates the open state of ChR2 C128T (Fig. 1 [5,6,10,11]).

The difference map between these two states revealed three prominent negative difference peaks near TMH2, TMH6 and TMH7, indicating a significant reorientation or rearrangement of these helices. The negative peak close to TMH6 was accompanied by a similarly sized positive peak, revealing an outward tilt movement by approximately 2 Å. The strong negative peak at TMH7 was accompanied by a broad positive peak on one side and a smaller positive peak on the other side, suggesting both a loss of order and a slight inward tilt. The third strong negative peak at TMH2 was not accompanied by a positive peak, indicating a loss of density, rather than a shift or reorientation of this helix. No significant differences were observed near TMH1 and TMH5 or the dimer interface helices TMH3 and TMH4.

Under physiological conditions, cations pass the ChR2 channel in the conductive state from the extracellular side to the intracellular side. The C1C2 structure [7,13] shows a possible cation-conducting pathway formed by TMH1, TMH2, TMH3 and TMH7. Compared to bacteriorhodopsin (bR), the light-driven archaeal proton pump, TMH1 and TMH2 are tilted outward in the closed state, thereby enlarging a vestibule of the putative channel. A change in water content in the channel during the photocycle was inferred from Fourier transform infrared data and discussed as one of the mechanism controlling cation permeation [8,14,15], as in K^+ channels [9,16]. Cations appear to enter the channel through the extracellular vestibule with several polar residues, including a series of conserved glutamates in TMH2. In the C1C2 structure, the putative pore is open at the extracellular side, whereas it is occluded by two constrictions near the cytoplasmic side.

The first of these constrictions is formed by the three conserved polar residues Ser102 (63 in ChR2), Glu129 (90) and Asn297 (258), which were shown to affect ion selectivity and channel kinetics, if replaced by Asp, Ala or Asp, respectively [4,10,11,13]. In a recent molecular dynamics study
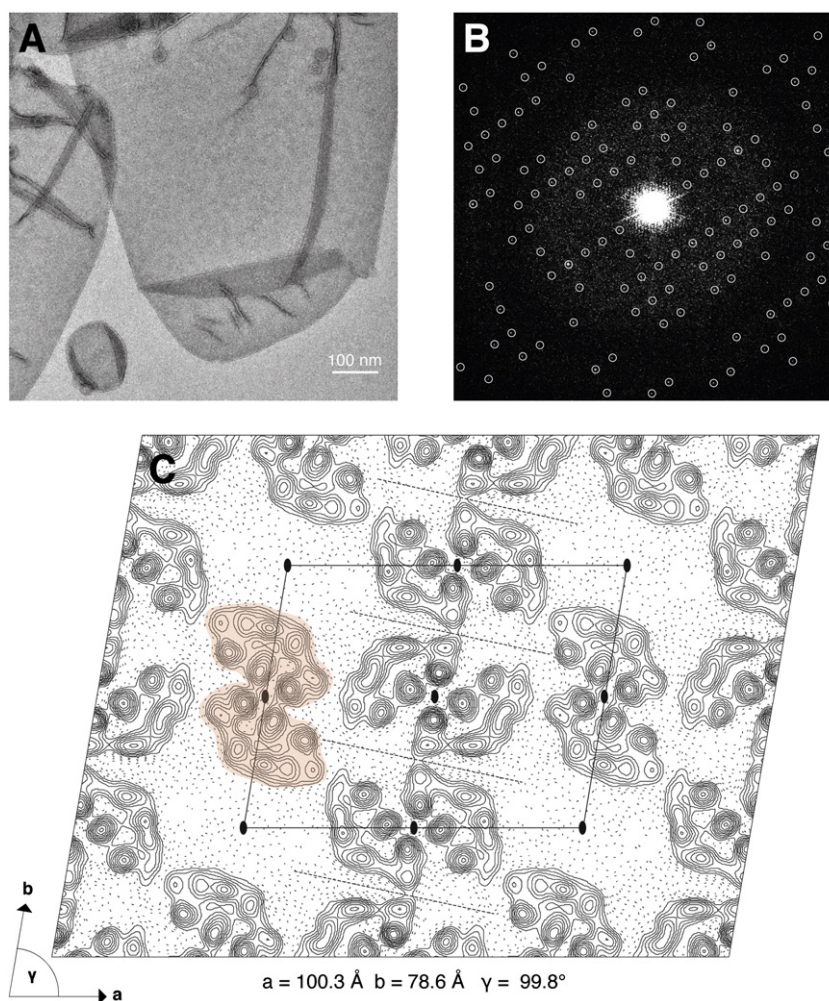
Fig. 2. Electron crystallography of C128T ChR2. (A) Negatively stained 2D crystals are flattened tubular vesicles. (B) Fourier transform of a distortion-corrected micrograph of an unstained crystalline vesicle taken at 4 K. Diffraction spots from one of the two crystalline layers are circled. (C) Projection map calculated to 6 Å resolution with applied *p*2 symmetry (phases constrained to 0° or 180°). One ChR2 dimer is shown in orange. Black ovals indicate crystallographic 2-fold axes; broken lines indicate non-crystallographic in-plane 2-fold axes. Contour lines above the mean density are continuous. The maximum density was scaled to 250 and contoured in steps of 25. No temperature factor was applied.

[17], a discontinuity in the distribution of water molecules between the cytoplasmic and extracellular sides was observed at this constriction site. The second constriction is formed by the phenol group of Tyr109 (70).

The large single difference peak at TMH2 (Fig. 4A) indicates significant changes in the protein backbone of this helix, such as a partial unwinding, during light activation. Comparison with similar work on bR [7] suggested that this is likely to occur at the cytoplasmic end of TMH2, which is therefore more ordered in the ground state than in the conductive open state. A loss of order in the cytoplasmic part of TMH2 would be an extension of the unresolved loop between TMH1 and TMH2 in the C1C2 structure and it could widen the channel in this region, creating a cytoplasmic vestibule next to the second constriction

site, which would allow cations to pass through the channel.

TMH2 contains a cluster of five conserved glutamates (81, 82, 90, 97 and 101). Glu90, Glu97 and Glu101 (Glu129, Glu136 and Glu140 in C1C2) are pointing toward the protein interior, thereby lining the putative channel. This chain of negative charges might allow water molecules to form a wire-like arrangement, as proposed by the molecular dynamics study [17]. Replacing Glu90, Glu97 and Glu101 in ChR2 by positively charged or non-polar residues modulated the ion selectivity and conductance of ChR2 [14,18–20]. In particular, the central Glu90 affects ion selectivity and its mutation is one of the factors turning ChR even into an anion-permeable channel [21,22]. Sequence alignment among all known ChRs reveals a high conservation of residues
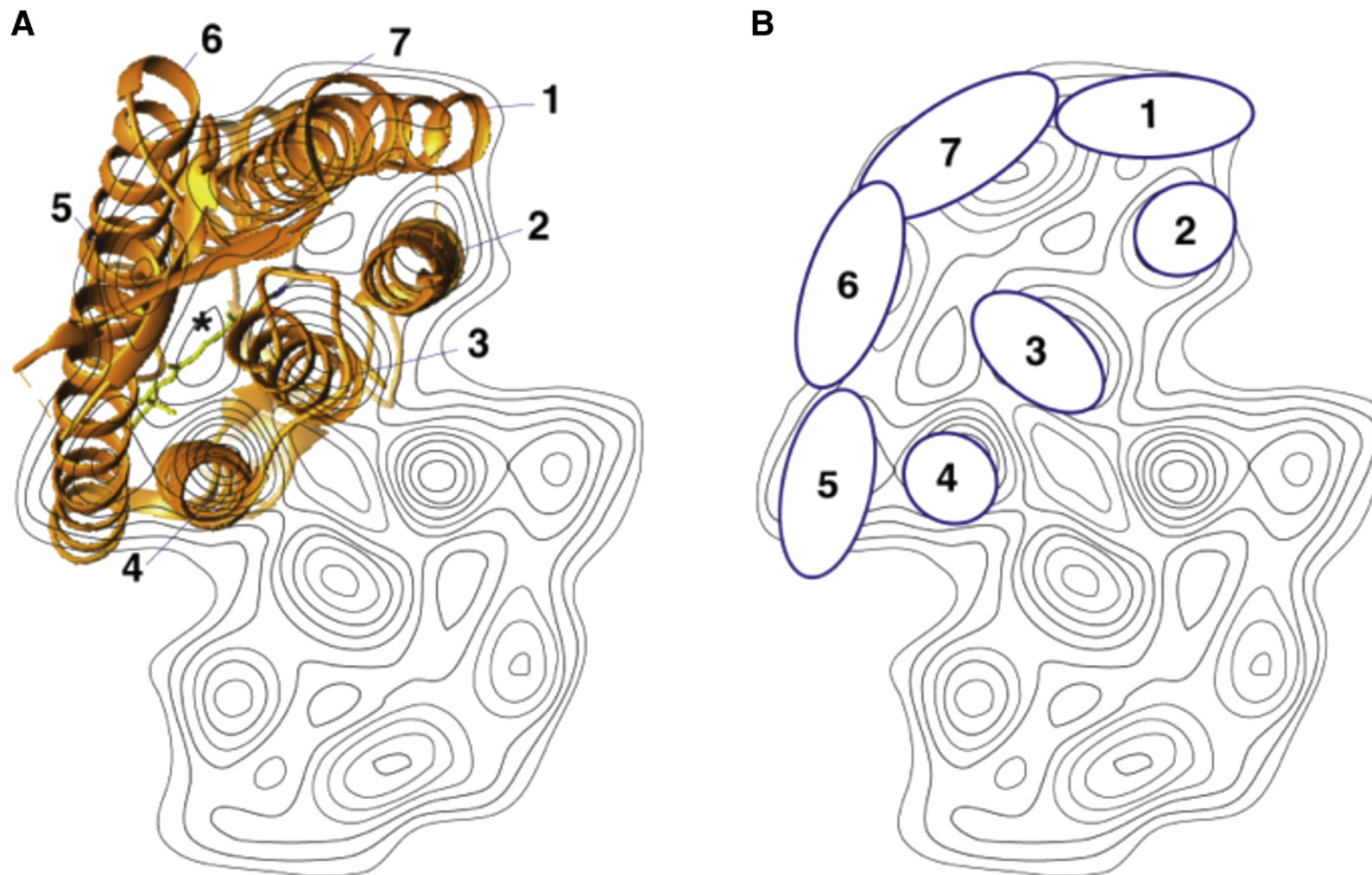
Fig. 3. Helix assignment in the 6-Å projection map of ChR2 C128T. (A) Superposition of one C1C2 protomer (3UG9, orange [13]) on the ChR2 projection map. Asterisk: position of the all-*trans* retinal. (B) Projections of TMH1–TMH7 are shown as ovals.
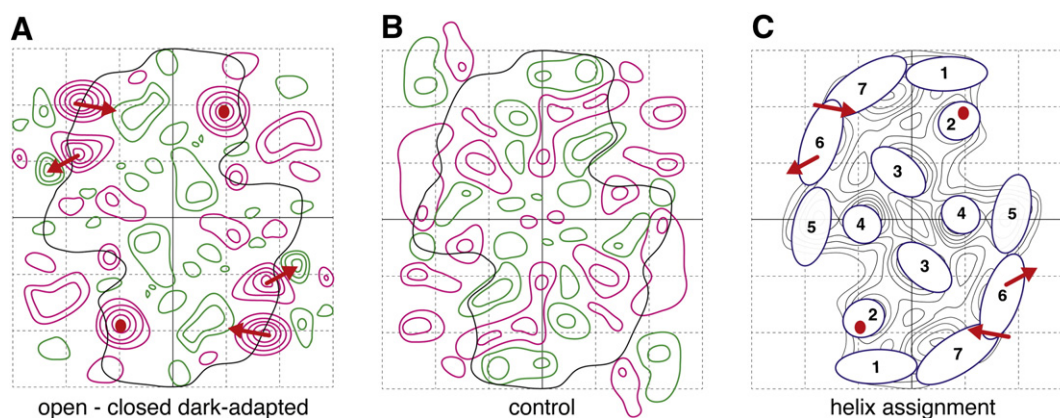
Fig. 4. Light-induced conformational changes in C128T ChR2. (A and B) Difference maps indicate the location and extent of light-induced conformational changes. The continuous black line marks the ChR2 dimer. Positive contours are shown in green; negative contours are shown in magenta. (A) Differences between crystals trapped after illumination (open state) and dark-adapted crystals (closed state). (B) Control difference map providing an estimate of background noise (two standard deviations) was generated from the 473-nm data divided into two equal halves. To enhance the signal-to-noise ratio, we applied non-crystallographic averaging of the three asymmetric units prior to calculating difference maps. (C) Helix assignment in the ChR2 dimer as in (B). Red arrows: putative helix movements. All maps are viewed from the cytoplasmic side. The maximum density of the maps was scaled to 500 and contoured in steps of 50.

Glu82, Glu90 in TMH2 and Arg268 in TMH7. Upon photoisomerization, a salt bridge between Glu82/Arg268 and a hydrogen bond between Glu90/Asn258 might relay conformational changes from TMH7 to TMH2, as the salt bridge between the Schiff base and the initial proton acceptor D253 in TMH7 is disrupted [15].

Fourier transform infrared spectroscopy of wild-type ChR2 [23,24] and the C128T mutant [24] indicated that light-induced conformational changes were both larger and different from those observed in bR, halorhodopsin (HR) and sensory rhodopsin II (SRII), as would be necessary to facilitate the passage of large cations, such as guanidinium [1]. It was suggested that formation of the early ChR2 photointermediate is accompanied by significant alterations in protein secondary structure, which persist throughout the conductive state [24]. The partial unwinding of TMH2 that we observe upon photoactivation would account for this finding.

Recent electron paramagnetic resonance (EPR) studies by double electron–electron resonance were conducted with wild-type ChR2 [25] and C128T mutant [26] using a spin label attached to a native cysteine at the cytoplasmic sides of TMH2 (Cys79) and TMH6 (Cys208). With both the wild-type protein and the mutant, the same light-induced increase in the average distance between the Cys79 in the two protomers was observed, indicating an outward movement of Cys79, which was attributed to a shift or reorientation of TMH2, or of the flexible loop connecting this helix to TMH1. Distance changes associated with TMH6 could not be assessed quantitatively for the wild type [25] but were suggested for the C128T mutant [26]. The move-

ment of TMH7 was not investigated by EPR due to the lack of a suitable cysteine in this helix. These results are consistent with our finding that TMH2 is conformationally active. In addition, we observe difference peaks at TMH6 and TMH7, indicating a tilt of these helices not detected by the EPR study.

Light-induced differences in the location of TMH6 and TMH7 of ChR2 are consistent with similar movements of the corresponding helices in bR [7,27], SRII [28–31] and HR [32], which are thus a common feature of conformational dynamics in microbial-type rhodopsins. However, in the complex of SRII with its transducer, the TMH6 movement is inhibited and replaced by a rotation of one of the transducer TMHs [29,33]. The pronounced change of TMH2 observed both by us and in the double electron–electron resonance study adds a new mode of rhodopsin dynamics to the well-documented displacement of the corresponding helix F in bR, SRII and HR. We conclude that conformational changes in this region of the protein constitute a key structural element of ChR2.

The pair of negative/positive peaks close to TMH6 is similar to the observed movement of the corresponding helix F in bR [7,27], which is linked to the conformational change upon retinal isomerization in helix G (TMH7 in ChR2). In bR, this has been suggested to be part of the mechanism that resets the pump by facilitating reprotonation of the Schiff base by allowing water molecules to enter the channel region [27]. The prominent negative difference peak at TMH7 indicates a loss of order in this helix upon photoisomerization of the attached retinal, which might contribute to channel opening. The opposite effect was observed for helix G in bR

Table 1. Crystallographic image statistics

Data set/condition	Unit cell parameters	Plane group symmetry[a]	No. of images/no. of experiments	Range of defocus (μm)	Resolution range (Å)	No. of unique reflections[b]	Phase residual[c] (°) (*versus* 0/180°, random = 45°)
Open/t = 0.5 s, λ_b = 473 nm	a = 100.3 ± 0.7 Å b = 78.6 ± 0.5 Å γ = 99.8 ± 0.2°	$p2$	16/5	0.6–1.4	> 14.7	56	15.0
					14.7–10.4	59	16.7
					10.4–8.5	54	17.5
					8.5–7.4	57	30.4
					7.4–6.6	52	34.3
					6.6–6.0	56	39.8
					>6.0	$\sum$334	Overall: 25.5
Closed dark adapted/λ_r = ~750 nm	a = 100.3 ± 0.3 Å b = 78.6 ± 0.1 Å γ = 99.8 ± 0.2°		16/5	0.6–1.4	> 14.7	56	6.7
					14.7–10.4	59	14.2
					10.4–8.5	54	19.1
					8.5–7.4	57	28.5
					7.4–6.6	54	31.3
					6.6–6.0	59	38.3
					>6.0	$\sum$339	Overall: 24.8

[a] Symmetry as determined by the program ALLSPACE [50].
[b] Including reflections IQ ≤ 5–6 Å.
[c] Weighted amplitudes and averaged phase residuals that show the phase deviation from theoretical 0°/180° (45 is random).

[34], which was found to become more ordered in the M state. EPR indicated an inward movement of helix F by ~ 1 Å later in the bR photocycle [27]. The broad positive peak in our difference next to TMH7 map suggests a similar inward movement of this helix in ChR2.

How do the TMH movements we observe relate to the function of ChR2? It was demonstrated before that ChR2 works both as an ion channel and as a proton pump [35]. As in other proton-pumping rhodopsins such as bR or SRII, changes in TMH6 and TMH7 might control the proton uptake that is required for the reprotonation of D156 that acts as the proton donor for the Schiff base in ChR2 [15]. On the other hand, the observed changes in TMH2 seem to be involved in cation permeation through the pore. Hence, our structural results might provide a structural framework for the dual functionality of ChR2 so that the protonation reactions associated with the photocycle intermediates are decoupled from cation permeation through the channel. Both reactions require different ion pathways in the same seven-helix protomer.

In summary, we trapped and characterized the open and closed states of ChR2 in the photocycle. We demonstrate that the transition from the closed state to the open state is linked to light-induced tilt movements of TMH6 and TMH7, plus a loss of order in TMH2. We propose that these conformational changes create a water-filled conducting pore, as would be required for the conductance of up to 2000 ions per photocycle. Our approach sets the stage for studying the structural changes accompanying the formation and decay of other photocycle intermediates in ChR2. Future studies will aim at three-dimensional maps of the open and closed states at higher resolution and the temporal sequence of the helical dynamics.

Materials and Methods

Experimental design

Trapping conformational changes of C128T ChR2

Our experiment to trap the open state of ChR2 on EM grids was designed on the basis of previous work on the C128T mutant. The DC-gate mutants, which include C128T, have complex photocycles with slower opening and closing kinetics [10,11,24,36,37]. The insights derived from electrophysiological recordings are summarized in Fig. 1, which shows that the open state accumulates upon irradiation with blue light [10,11,24,36,37]. In the case of wild-type ChR2, the lifetime of the open state is too short-lived for our trapping design (~ 30 ms at 10 °C [35]). Replacement of C128T prolongs the lifetime of the open state to ~ 2 s at 20 °C [10,11]. Hence, a short blue-light illumination of 0.5 s will accumulate mainly the open state that is freeze-trapped in liquid nitrogen (Fig. 1). Furthermore, our protocol avoids other photointermediates associated with the desensitized state of the channel or other side products that are populated under continuous illumination [36,38].

Sample preparation

The sample environment prior to light activation and freezing was maintained at 4 °C. 2D crystals of C128T ChR2 were prepared in trehalose, which preserves the internal protein structure for cryo-EM [39–41]. To ensure that the medium was sufficiently fluid for ChR2 to undergo conformational changes, we kept the relative humidity at ~ 80% throughout the experiment [42].

Expression and purification of ChR2 in *Pichia pastoris*

The cDNA of *chop2* (GenBank accession number AF461397) encoding residues 1–315 of ChR2 plus a

C-terminal His9 tag sequence was cloned in the pPIC9K vector (Invitrogen) using restriction enzymes EcoRI and NotI. The C128T mutant [11] was generated with the QuikChange kit (Stratagene) and confirmed by sequence analysis. The pPIC9K-chop2(1–315)His9 vector was linearized and transformed into *P. pastoris* strain SMD1163 (*his4*, *pep4*, *prB1*; Invitrogen). Cells were grown, and membranes were prepared as previously described [43] with modifications [11].

2D crystallization

The C128T ChR2 mutant was mixed with 1,2-dimyristoyl-*sn*-glycero-3-phosphocholine (Avanti Polar Lipids, Inc., USA) solubilized in 2% *n*-decyl-β-D-maltopyranoside (Glycon Biochemicals) at a lipid-to-protein ratio of 1.25 (wt/wt) and a final protein concentration of 1 mg/ml. The mixture was incubated at room temperature for 30 min before being transferred to dialysis buttons. 2D crystals were grown in 50-μl buttons sealed with dialysis membranes (25 kDa molecular mass cutoff) against 100 ml buffer (20 mM Hepes, pH 7.4, 100 mM NaCl, 10 mM MgCl₂, 20% glycerol and 3 mM NaN₃) at 28 °C for 2 weeks. Buffer was exchanged every 3 days. Dialysis vessels were wrapped in aluminum foil. 2D crystals of ChR2 were stable for several months.

Electron microscopy

Negative staining and screening

The morphology and quality of 2D crystals was assessed by negative-stain EM. Samples (5 μl) were adsorbed to a 400-mesh carbon-coated copper grid for 5 s, washed three times in distilled water, stained with 0.5% uranyl acetate and examined in a Philips CM120 electron microscope at 120 kV acceleration voltage.

Preparation of laser-flashed 2D crystals for cryo-EM

To trap light-induced conformational changes in ChR2, we designed a plunge-freezing apparatus operated by pressurized nitrogen gas and interfaced with a laser to irradiate the 2D crystals on the EM grid prior to freezing (Fig. 1). 2D crystals were kept in the dark for 12 h and were then prepared for cryo-EM under red light (λ_r = 750 nm; Ilford safelight filter 904) at 4 °C and ~80% relative humidity. EM grids of tubular 2D crystals were prepared with 1–2 μl of crystal suspension by the back-injection method [44] in 5% trehalose on carbon-coated copper grids. Excess buffer was blotted off with a wedge of no. 4 Whatmann filter paper, and the grid was mounted in the cryo-plunger.

Prior to irradiation, the laser beam was adjusted perpendicular to the surface of the EM grid for optimal excitation of the retinylidene chromophores, which are oriented parallel to the grid plane. The beam diameter was expanded to cover the entire grid area. Grids were irradiated with laser flashes from a diode-pumped solid-state laser (Pusch OptoTech GmbH) at a light intensity between 1 and 13 mW/mm². The duration of the light pulses was set by a fast computer-controlled shutter (Uniblitz LS6ZM2, Vincent Associates) coupled to the plunger release mechanism with ~10 ms delay.

For trapping the open conformation of ChR2, we irradiated crystals with light from a blue laser (λ_b = 473 nm) for *t* = 0.5 s. The closed, dark-adapted conformation was obtained under constant red light (λ_r = 750 nm) without laser flashes under otherwise identical conditions.

Upon release of the plunger, the grid was injected into a bath of liquid nitrogen. Under the conditions of our experiment, the cooling rate of the specimen is ~5000 K/s [45]. Hence, the sample temperature should equilibrate with the bath temperature of 77 K within 50–100 ms after immersion in liquid nitrogen. Spectroscopic data showed that the first spectral intermediate after the isomerization can be trapped at 80 K [23,24]. Therefore, we argue that all further transitions are also not thermally accessible at this temperature. All subsequent handling of the specimen, including cryo-transfer and cryo-EM, was carried out at liquid nitrogen temperature. For each condition, five independent experiments were performed; for details, see Table 1.

The plunger speed of 10 mm/ms and the distance of 80 mm above the liquid nitrogen surface resulted in an 8-ms delay before freezing after the light flash. Together with the 10-ms delay of the release mechanism and the freezing rate in liquid nitrogen, we estimate a maximum of ~620 ms from the start of irradiation to the point where the sample is frozen. After this time, the majority of the molecules are in the open state, while our illumination protocol should prevent the accumulation of side products that occurs under continuous illumination with blue light [37]. Our experimental conditions thus meet the requirements for trapping the open state of the slow C128T mutant.

Data collection and processing

2D crystals were imaged in a JEOL 3000 SFF helium-cooled electron microscope equipped with a field emission gun at 4 K at an acceleration voltage of 300 kV. Images were recorded by the spot-scan procedure with an electron dose of 20–30 e/Å² on Kodak SO-163 film at a nominal magnification of 60,000× and an exposure time ranging from 30 to 40 ms per spot. Films were developed for 12 min in full-strength Kodak D19 developer. The quality of negatives was evaluated by optical diffraction and those exhibiting strong reflections to 10 Å were selected for further processing.

Micrographs were digitized with a Zeiss SCAI scanner using a step size of 7 μm, corresponding to 1.3 Å at the specimen. The 2dx [46,47] and MRC [48] software packages were used for image processing and data merging. Projection maps were calculated with the CCP4 program suite [49]. The plane group symmetry of the crystals was determined using the program ALLSPACE by comparing phases of symmetry-related reflections [50].

Difference maps

Difference maps were calculated from phases and amplitudes of structure factors obtained at different stages of the ChR2 photocycle using scripts from the CCP4 program suite [49]. Projection phases and amplitudes for each data set were calculated using the 2dx software, scaled (sftools) and subtracted by vector subtraction in reciprocal space (overlapmap). Scaled amplitudes and phases for the closed dark-adapted conformation were subtracted from the corresponding data obtained for the open conformation.

As a control (Fig. 4B), difference maps were calculated from data obtained at the same conditions, randomly divided into two halves. These control difference map provided an estimate of background noise, which was about two standard deviations.

Non-crystallographic symmetry averaging

Non-crystallographic symmetry was applied in real space using the CCP4 routines MAPROT, MAPMASK and NPO, which resulted in an average of the three asymmetric units in the unit cell.

References

[1] Nagel G, Szellas T, Huhn W, Kateriya S, Adeishvili N, Berthold P, et al. Channelrhodopsin-2, a directly light-gated cation-selective membrane channel. Proc Natl Acad Sci U S A 2003;100:13940–5.

[2] Grote M, Engelhard M, Hegemann P. Of ion pumps, sensors and channels—perspectives on microbial rhodopsins between science and history. Biochim Biophys Acta 2014;1837:533–45.

[3] Spudich JL, Sineshchekov OA, Govorunova EG. Mechanism divergence in microbial rhodopsins. Biochim Biophys Acta 2014;1837:546–52.

[4] Lórenz-Fonfría VA, Heberle J. Channelrhodopsin unchained: structure and mechanism of a light-gated cation channel. Biochim Biophys Acta 2014;1837:626–42.

[5] Fenno L, Yizhar O, Deisseroth K. The development and application of optogenetics. Annu Rev Neurosci 2011;34:389–412.

[6] Miesenböck G. Optogenetic control of cells and circuits. Annu Rev Cell Dev Biol 2011;27:731–58.

[7] Subramaniam S, Gerstein M, Oesterhelt D, Henderson R. Electron diffraction analysis of structural changes in the photocycle of bacteriorhodopsin. EMBO J 1993;12:1–8.

[8] Unwin N. Acetylcholine receptor channel imaged in the open state. Nature 1995;373:37–43.

[9] Paulino C, Kühlbrandt W. pH- and sodium-induced changes in a sodium/proton antiporter. eLife 2013;3:e01412-2.

[10] Berndt A, Yizhar O, Gunaydin LA, Hegemann P, Deisseroth K. Bi-stable neural state switches. Nat Neurosci 2009;12:229–34.

[11] Bamann C, Gueta R, Kleinlogel S, Nagel G, Bamberg E. Structural guidance of the photocycle of channelrhodopsin-2 by an interhelical hydrogen bond. Biochemistry 2010;49:267–78.

[12] Müller M, Bamann C, Bamberg E, Kühlbrandt W. Projection structure of channelrhodopsin-2 at 6 Å resolution by electron crystallography. J Mol Biol 2011;414:86–95.

[13] Kato HE, Zhang F, Yizhar O, Ramakrishnan C, Nishizawa T, Hirata K, et al. Crystal structure of the channelrhodopsin light-gated cation channel. Nature 2012;482:369–74.

[14] Eisenhauer K, Kuhne J, Ritter E, Berndt A, Wolf S, Freier E, et al. In channelrhodopsin-2 Glu-90 is crucial for ion selectivity and is deprotonated during the photocycle. J Biol Chem 2012;287:6904–11.

[15] Lórenz-Fonfría VA, Resler T, Krause N, Nack M, Gossing M, Mollard von GF, et al. Transient protonation changes in channelrhodopsin-2 and their relevance to channel gating. Proc Natl Acad Sci 2013;110:E1273–81.

[16] Jensen MØ, Borhani DW, Lindorff-Larsen K, Maragakis P, Jogini V, Eastwood MP, et al. Principles of conduction and hydrophobic gating in K$^+$ channels. Proc Natl Acad Sci 2010;107:5833–8.

[17] Watanabe HC, Welke K, Sindhikara DJ, Hegemann P, Elstner M. Towards an understanding of channelrhodopsin function: simulations lead to novel insights of the channel mechanism. J Mol Biol 2013;425:1795–814.

[18] Sugiyama Y, Wang H, Hikima T, Sato M, Kuroda J, Takahashi T, et al. Photocurrent attenuation by a single polar-to-nonpolar point mutation of channelrhodopsin-2. Photochem Photobiol Sci 2009;8:328–36.

[19] Gradmann D, Berndt A, Schneider F, Hegemann P. Rectification of the channelrhodopsin early conductance. Biophys J 2011;101:1057–68.

[20] Ruffert K, Himmel B, Lall D, Bamann C, Bamberg E, Betz H, et al. Glutamate residue 90 in the predicted transmembrane domain 2 is crucial for cation flux through channelrhodopsin 2. Biochem Biophys Res Commun 2011;410:737–43.

[21] Berndt A, Lee SY, Ramakrishnan C, Deisseroth K. Structure-guided transformation of channelrhodopsin into a light-activated chloride channel. Science 2014;344:420–4.

[22] Wietek J, Wiegert JS, Adeishvili N, Schneider F, Watanabe H, Tsunoda SP, et al. Conversion of channelrhodopsin into a light-gated chloride channel. Science (New York NY) 2014; 344:409–12.

[23] Ritter E, Stehfest K, Berndt A, Hegemann P, Bartl FJ. Monitoring light-induced structural changes of channelrhodopsin-2 by UV-visible and Fourier transform infrared spectroscopy. J Biochem 2008;283:35033–41.

[24] Radu I, Bamann C, Nack M, Nagel G, Bamberg E, Heberle J. Conformational changes of channelrhodopsin-2. J Am Chem Soc 2009;131:7313–9.

[25] Sattig T, Rickert C, Bamberg E, Steinhoff H-J, Bamann C. Light-induced movement of the transmembrane helix B in channelrhodopsin-2. Angew Chem Int Ed Engl 2013;52:9705–8.

[26] Krause N, Engelhard C, Heberle J, Schlesinger R, Bittl R. Structural differences between the closed and open states of channelrhodopsin-2 as observed by EPR spectroscopy. FEBS Lett 2013;587:3309–13.

[27] Radzwill N, Gerwert K, Steinhoff HJ. Time-resolved detection of transient movement of helices F and G in doubly spin-labeled bacteriorhodopsin. Biophys J 2001;80:2856–66.

[28] Luecke H. Crystal structure of sensory rhodopsin II at 2.4 angstroms: insights into color tuning and transducer interaction. Science (New York NY) 2001;293:1499–503.

[29] Wegener AA, Klare JP, Engelhard M, Steinhoff HJ. Structural insights into the early steps of receptor-transducer signal transfer in archaeal phototaxis. EMBO J 2001;20:5312–9.

[30] Wegener AA, Chizhov I, Engelhard M, Steinhoff HJ. Time-resolved detection of transient movement of helix F in spin-labelled *Pharaonis* sensory rhodopsin II. J Mol Biol 2000;301: 881–91.

[31] Gushchin I, Reshetnyak A, Borshchevskiy V, Ishchenko A, Round E, Grudinin S, et al. Active state of sensory rhodopsin II: structural determinants for signal transfer and proton pumping. J Mol Biol 2011;412:591–600.

[32] Nakanishi T, Kanada S, Murakami M, Ihara K, Kouyama T. Large deformation of helix F during the photoreaction cycle of *Pharaonis* halorhodopsin in complex with azide. Biophys J 2013;104:377–85.

[33] Moukhametzianov R, Klare JP, Efremov R, Baeken C, Göppner A, Labahn J, et al. Development of the signal in sensory rhodopsin and its transfer to the cognate transducer. Nature 2006;440:115–9.

[34] Subramaniam S, Henderson R. Molecular mechanism of vectorial proton translocation by bacteriorhodopsin. Nature 2000;406:653–7.

[35] Feldbauer K, Zimmermann D, Pintschovius V, spitz J, Bamann C, Bamberg E. Channelrhodopsin-2 is a leaky proton pump. Proc Natl Acad Sci 2009;106:12317–22.

[36] Bamann C, Kirsch T, Nagel G, Bamberg E. Spectral characteristics of the photocycle of channelrhodopsin-2 and its implication for channel function. J Mol Biol 2008;375: 686–94.

[37] Ritter E, Piwowarski P, Hegemann P, Bartl FJ. Light-dark adaptation of channelrhodopsin C128T mutant. J Biol Chem 2013;288:10451–8.

[38] Stehfest K, Ritter E, Berndt A, Bartl F, Hegemann P. The branched photocycle of the slow-cycling channelrhodopsin-2 mutant C128T. J Mol Biol 2010;398:690–702.

[39] Crowe JH, Crowe LM, Chapman D. Preservation of membranes in anhydrobiotic organisms: the role of trehalose. Science (New York NY) 1984;223:701–3.

[40] Hirai TT, Murata KK, Mitsuoka KK, Kimura YY, Fujiyoshi YY. Trehalose embedding technique for high-resolution electron crystallography: application to structural study on bacteriorhodopsin. J Electron Microsc (Tokyo) 1998;48: 653–8.

[41] Jain NK, Roy I. Effect of trehalose on protein structure. Protein Sci 2008;18:24–36.

[42] Perkins GAG, Burkard FF, Liu EE, Glaeser RMR. Glucose alone does not completely hydrate bacteriorhodopsin in glucose-embedded purple membrane. J Microsc (Oxford) 1992;169:61–5.

[43] André N, Cherouati N, Prual C, Steffan T, Zeder-Lutz G, Magnin T, et al. Enhancing functional production of G protein-coupled receptors in *Pichia pastoris* to levels required for structural studies via a single expression screen. Protein Sci 2006;15:1115–26.

[44] Kühlbrandt W, Wang D. High-resolution electron crystallography of light-harvesting chlorophyll a/b-protein complex in three different media. J Mol Biol 1991;217:691–9.

[45] Echlin P. Low-temperature microscopy and analysis. Plenum Publishing Corporation; 1992.

[46] Gipson B, Zeng X, Stahlberg H. 2dx_merge: data management and merging for 2D crystal images. J Struct Biol 2007; 160:375–84.

[47] Gipson B, Zeng X, Zhang ZY, Stahlberg H. 2dx—user-friendly image processing for 2D crystals. J Struct Biol 2007; 157:64–72.

[48] Crowther RA, Henderson R, Smith JM. MRC image processing programs. J Struct Biol 1996;116:9–16.

[49] Bailey S. The CCP4 Suite—programs for protein crystallography. Acta Crystallogr Sect D Biol Crystallogr 1994;50: 760–3.

[50] Valpuesta JM, Valpuesta JM, Carrascosa JL, Carrascosa JL, Henderson R, Henderson R. Analysis of electron microscope images and electron diffraction patterns of thin crystals of phi 29 connectors in ice. J Mol Biol 1994;240:281–7.